Electronic Supplementary Material (ESI) for Inorganic Chemistry Frontiers.

Supplementary Information

Amorphous-crystalline $FeNi_2S_4$@NiFe-LDH nanograsses by molten salt as an industrially promising electrocatalyst for oxygen evolution

Fu-Li Wang, Xin-Yu Zhang, Jian-Cheng Zhou, Zhuo-Ning Shi, Bin Dong *,

Jing-Yi Xie, Yi-Wen Dong, Jian-Feng Yu, Yong-Ming Chai *

State Key Laboratory of Heavy Oil Processing, College of Chemistry & Chemical Engineering,

China University of Petroleum (East China), Qingdao 266580, PR China

∗ Corresponding author. Email: dongbin@upc.edu.cn (B. Dong); ymchai@upc.edu.cn (Y.M. Chai)

Tel: +86-532-86981156, Fax: +86-532-86981156

1. Experimental section

1.1. Characterizations

The X-ray powder diffraction (XRD) patterns were characterized by a JSM-7500F diffractometer produced by JEOL with Cu K α radiation (2° min^{-1} from 10° to 90°) to explore the relevant crystal structure. X-ray photoelectron spectroscopy (XPS) was measured by a VG ESCALABMK II system to analyze the chemical states of elements. The scanning electron microscopy (SEM) and SEM mapping analysis were performed with a Hitachi, S-4800 to investigated the morphology and element distribution. The high-resolution transmission electron microscopy (HRTEM) was carried out using a FEI Tecnai G2 F20 S-TWIN machine to observe more detailed lattice and structure information. The solid-liquid contact angle was investigated by an OCA20 machine. Electron paramagnetic resonance (EPR) was carried out by ADANI e-SPINOZA under the microwave power of 14 dB and modulation amplitude of 2.0 G. Inductively coupled plasma mass spectrometry (ICP-MS) characterization was adopt with a Thermo Fischer Scientific iCAP-QC. The N_2 adsorption−desorption experiment was measured on Quantachrome NOVA 4200e.

1.2. Electrochemical measurements

All the OER electrochemical measurement was performed with a electrochemical workstation (Gamry Reference 3000, USA) in a standard three-electrode system using $FeNi_2S_4$@NiFe-LDH as the working electrode, a Pt foil electrode as the counter electrode and saturated calomel electrode as the reference electrode. In order to simulate industrial conditions, 1 M KOH (25 °C) and 6 M KOH (70 °C) has been

used as electrolyte. Linear sweep voltammetry (LSV) was recorded at a scan rate of 2 mV s^{-1}, and the potential range was 0 - 0.7 V vs SCE. All potentials reported has been calibrated to reversible hydrogen electrode (RHE). When the electrolyte required was 1 M KOH (25 °C), the Nernst equation could be expressed as $E_{RHE} = E_{SCE} + 0.059pH + 0.245$. When the electrolyte required was 6 M KOH (70 °C), the pH value is 14.78 and the corresponding Nernst equation could be expressed as $E_{RHE} = E_{SCE} + 0.059pH + 0.219$. The electrochemical ohmic resistance (EIS) was evaluated at the potential of 0.4 V vs SCE. The electrochemical active surface areas (ECSAs) were calculated from electric double layer capacitance (C_{dl}) which was determined by the measurements of cyclic voltammetry (CV) in a potential range of 0.3 - 0.4 V (vs SCE) at a scan rate range of 5-20 mV s^{-1}. The ECSA is proportional to C_{dl} based on $ECSA=C_{dl}/C_s$, where C_s is the specific capacitance and is considered to be a constant, which is reported to be between 0.022 and 0.130 mF cm^{-2} in alkaline solution. In this study, we assumed the value of C_s to be 0.040 mF cm^{-2} in 1 M KOH. The stability test of catalysts was analyzed by a V-t curve, where the constant current was 400 and 500 cm^{-2}, respectively. The stability tests were conducted by three ways: (i) accelerating degradation test (ADT) for 5000 cycles at a scan rate of 40 mV s^{-1}, (ii) simulated intermittent condition by applied the current density from 200 until 1000 mA cm^{-2} with an increment of 100 mA cm^{-2} every 600 s and returned back to 200 mA cm^{-2}, (iii) chronopotentiometry measurement at a fixed current density of 500 mA cm^{-2} for 600 h.

Fig. S1

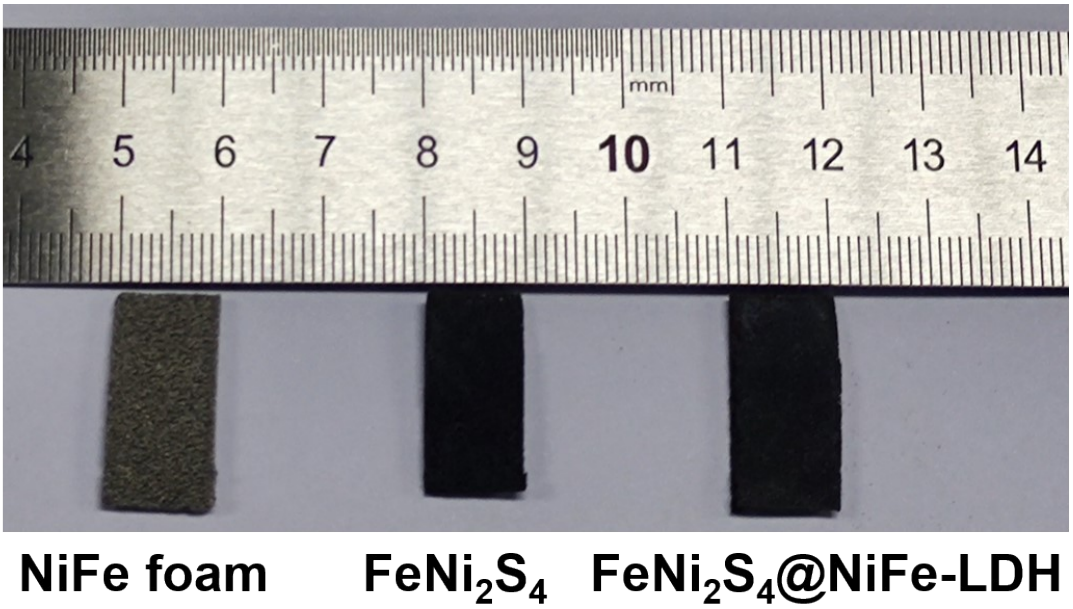

Fig. S1. Optical photograph (from left to right) of NiFe foam, $FeNi_2S_4$, $FeNi_2S_4$@NiFe-LDH.

Fig. S2

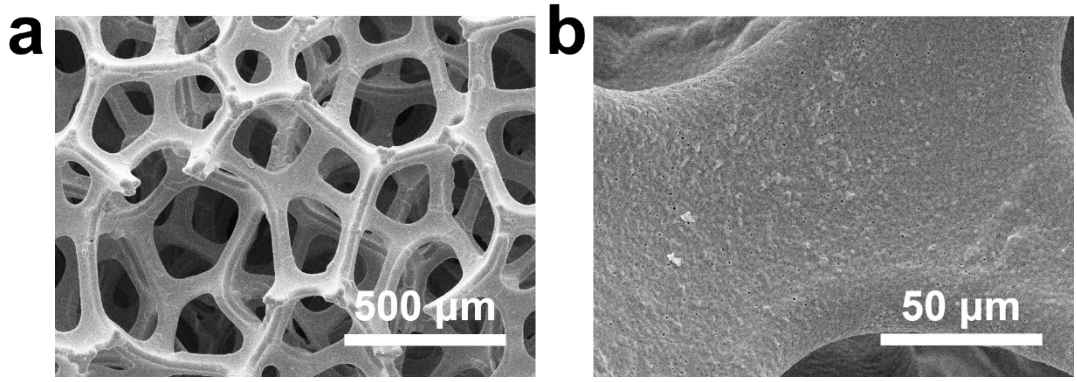

Fig. S2. SEM images of NiFe foam.

Fig. S3

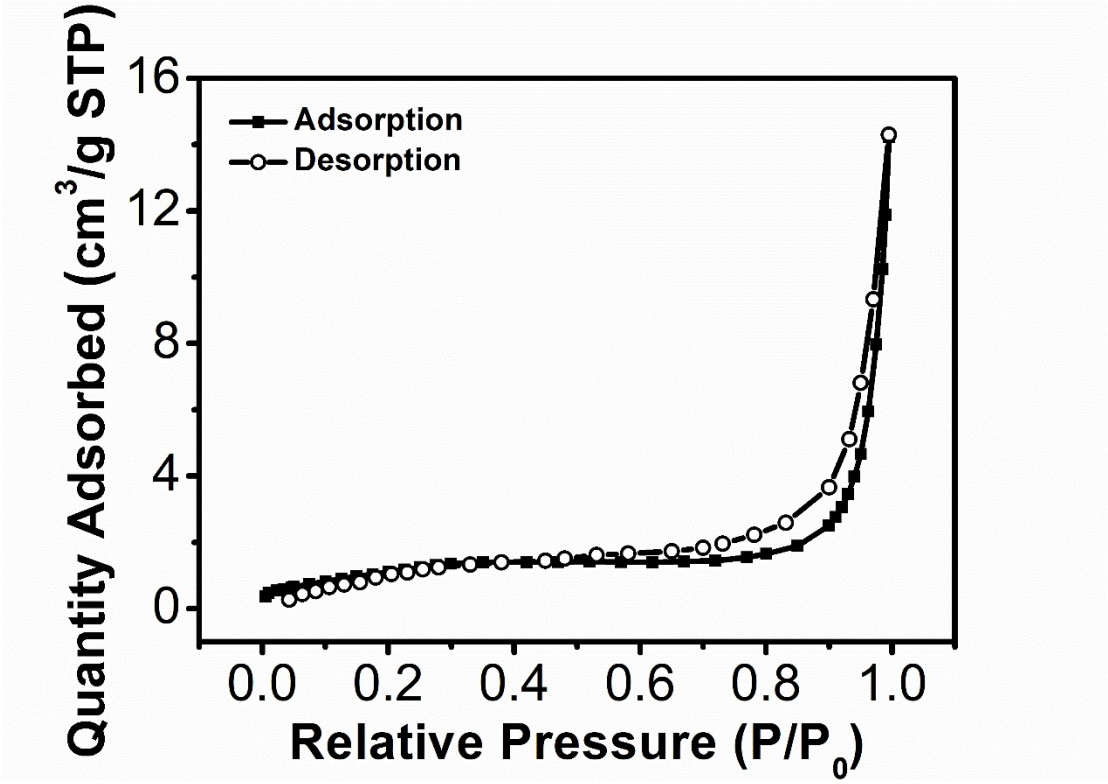

Fig. S3. N_2 adsorption-desorption isotherms of $FeNi_2S_4$@NiFe-LDH.

Fig. S4

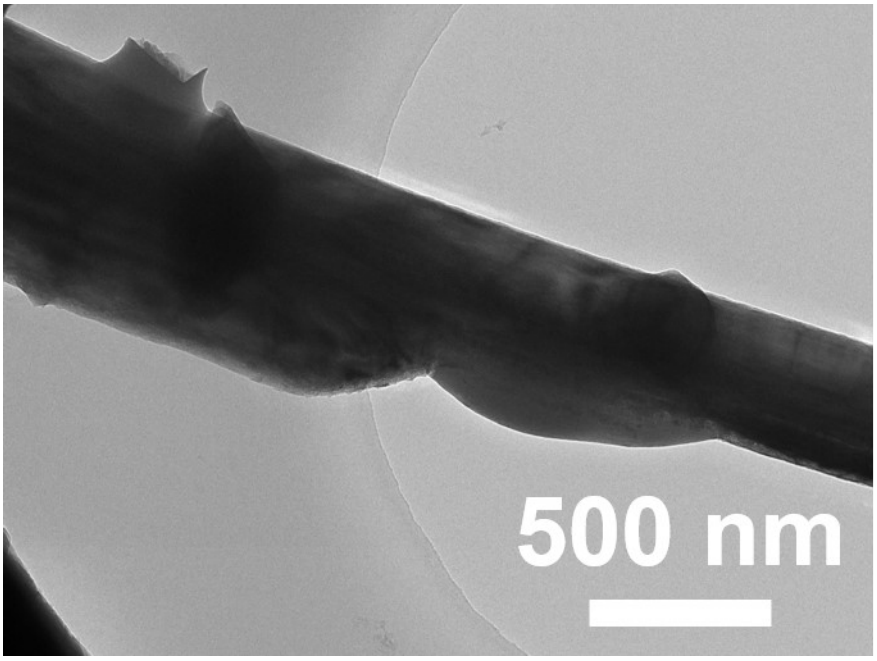

Fig. S4. TEM images of $FeNi_2S_4$.

Fig. S5

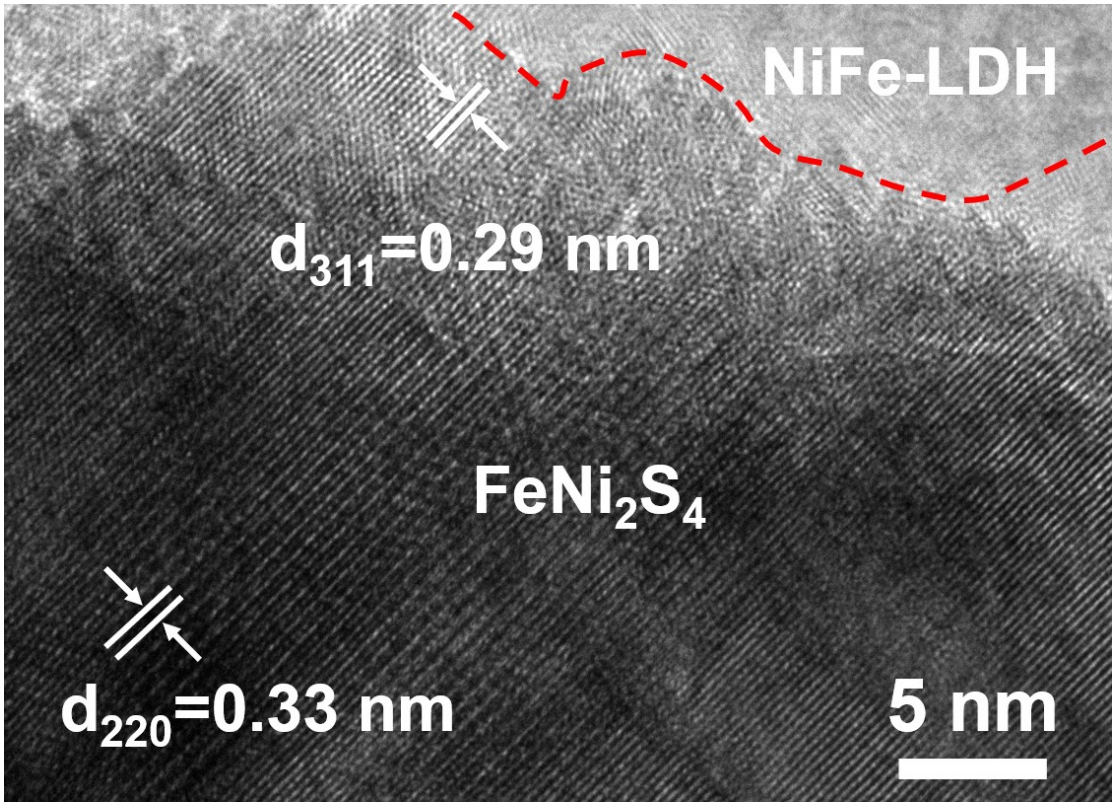

Fig. S5. high-resolution TEM images of $FeNi_2S_4$.

Fig. S6

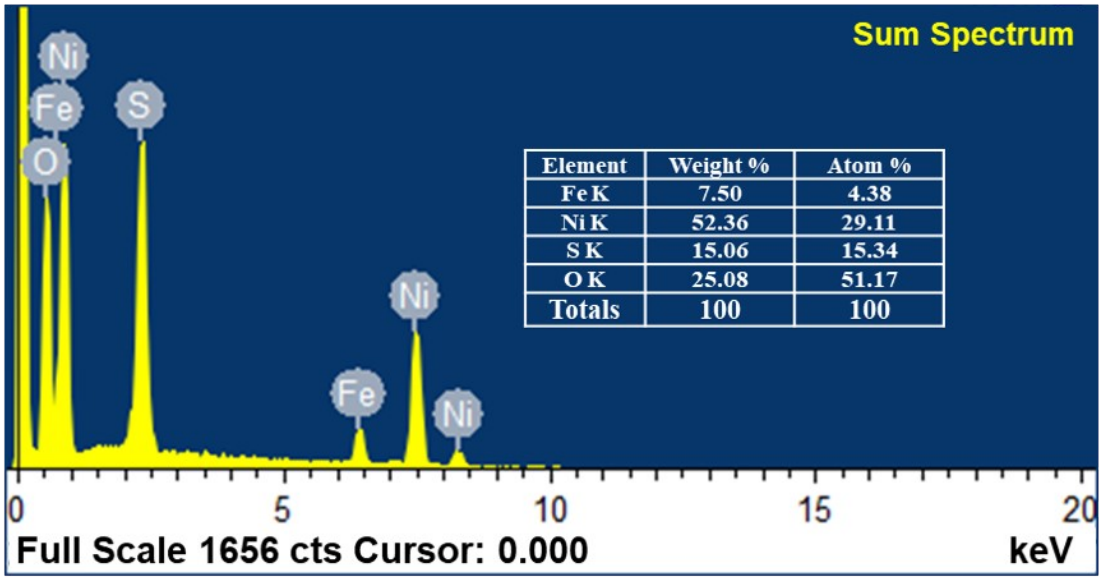

Fig. S6. SEM-EDX spectrum for the $FeNi_2S_4$@NiFe-LDH.

Fig. S7

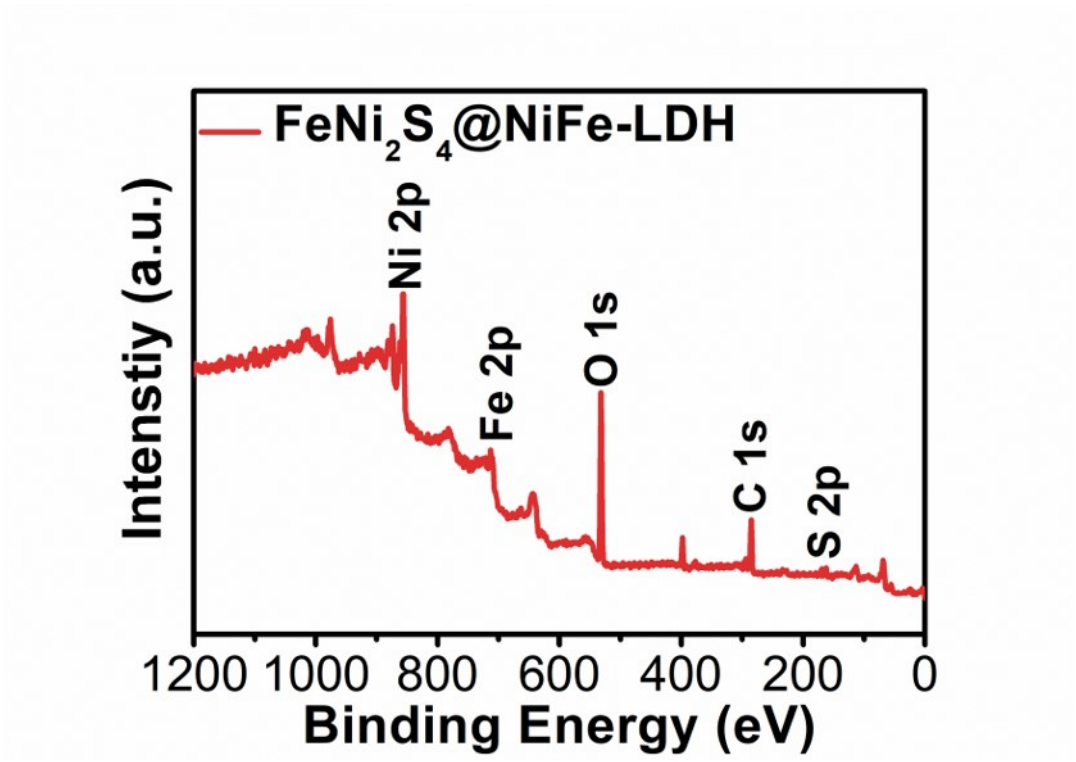

Fig. S7. overall XPS spectra for the $FeNi_2S_4$@NiFe-LDH.

Fig. S8

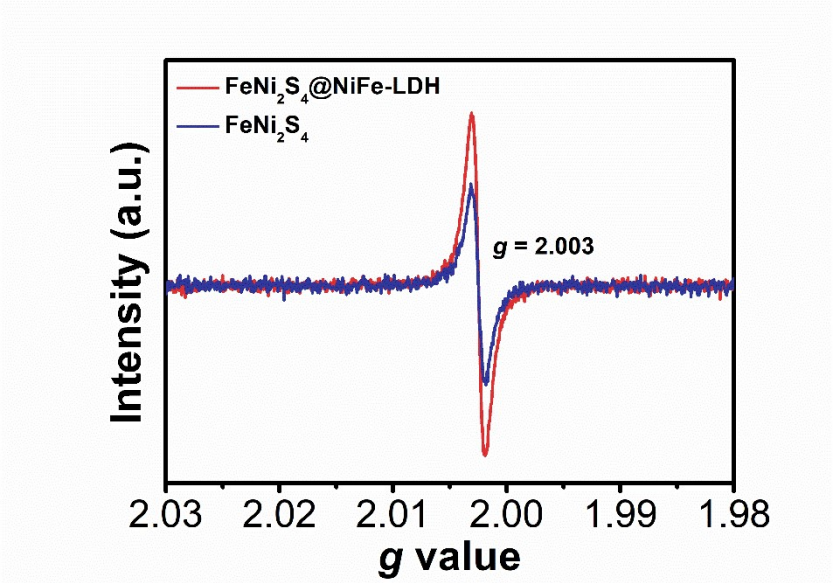

Fig. S8. The EPR spectra of powder $FeNi_2S_4$@NiFe-LDH and $FeNi_2S_4$ peeled off from the NiFe foam.

Fig. S9

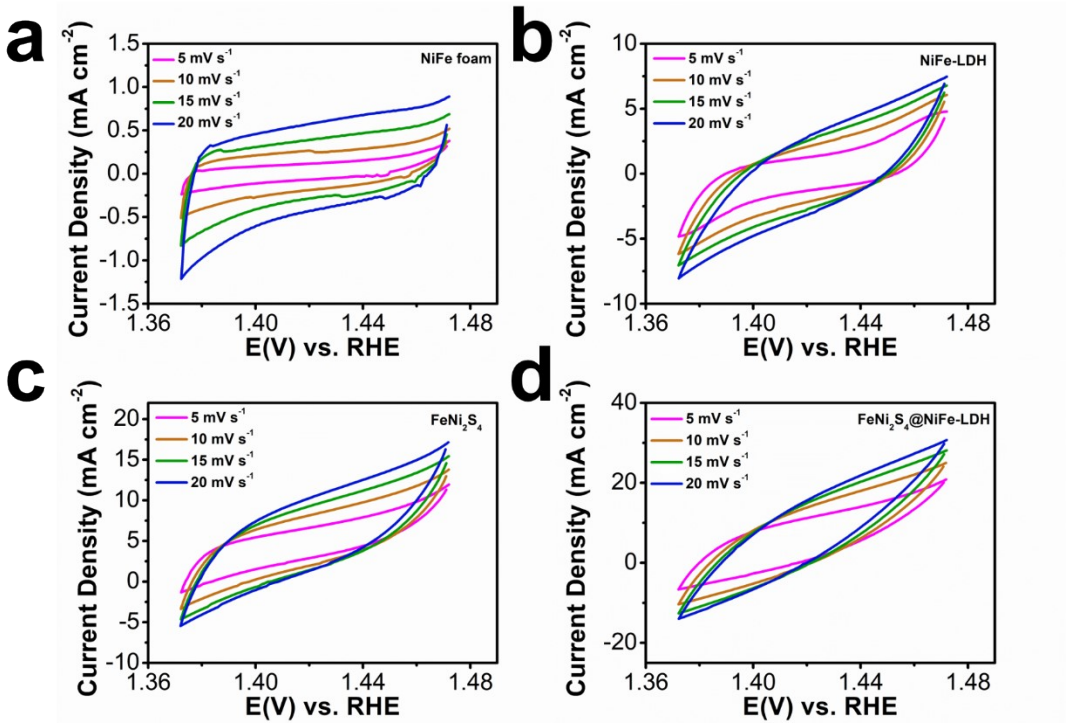

Fig. S9. Cyclic voltammetry curves (CVs) of NiFe foam (a), NiFe-LDH (b), $FeNi_2S_4$ (c) and $FeNi_2S_4$@NiFe-LDH (d) with different scanning rates (5, 10, 15, 20 mV s^{-1}) in the potential range of 1.37~ 1.47 V (vs. RHE).

Fig. S10

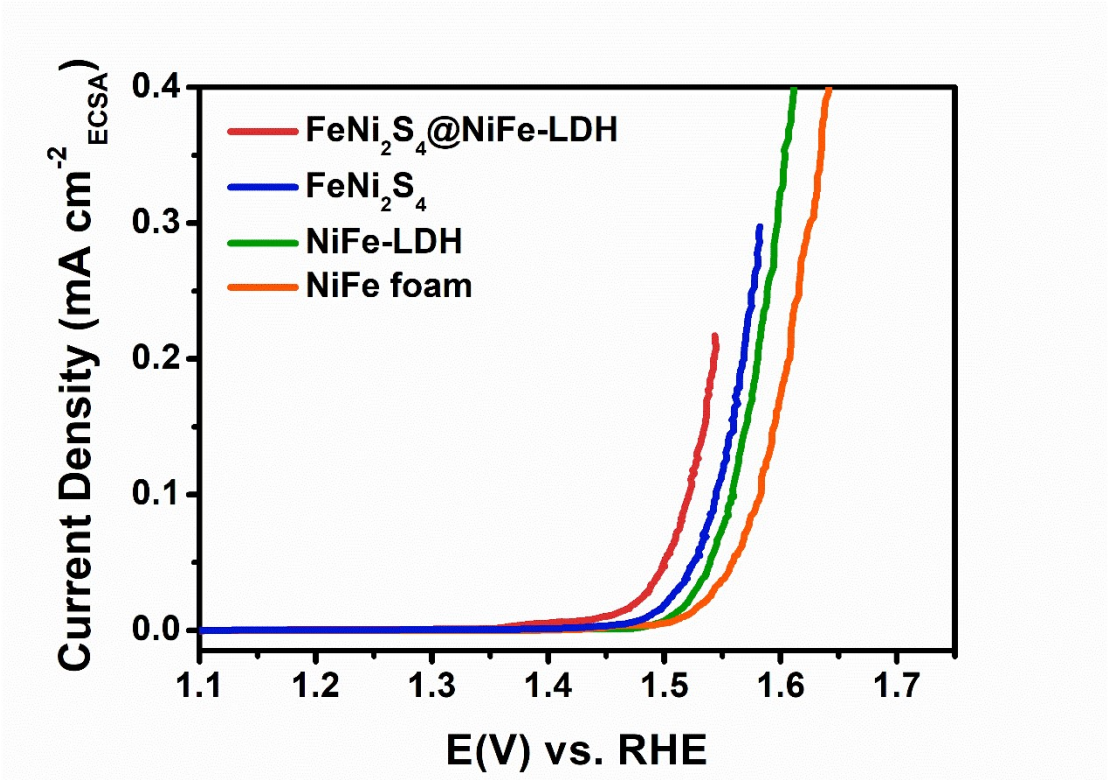

Fig. S10. OER polarization curves normalized by electrochemically active surface area (ECSA) for $FeNi_2S_4$@NiFe-LDH, $FeNi_2S_4$, NiFe-LDH and NiFe foam.

Fig. S11

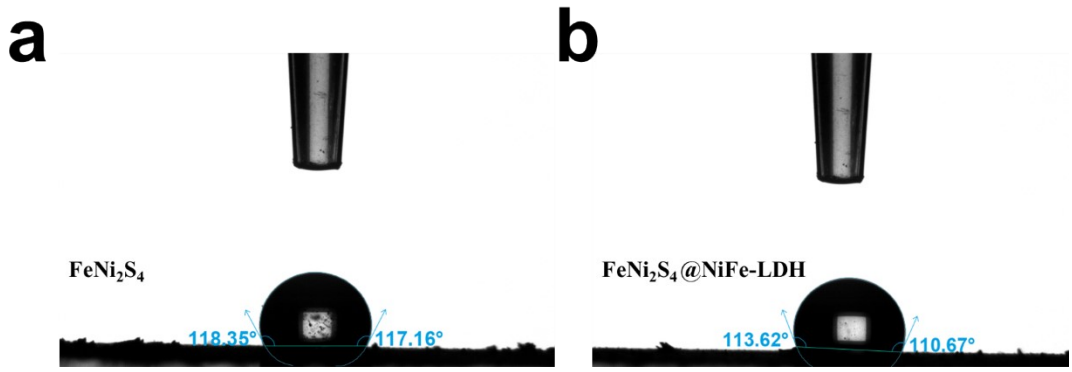

Fig. S11. The solid-liquid contact angles of (a) $FeNi_2S_4$ and (b) $FeNi_2S_4$ @NiFe-LDH.

Fig. S12

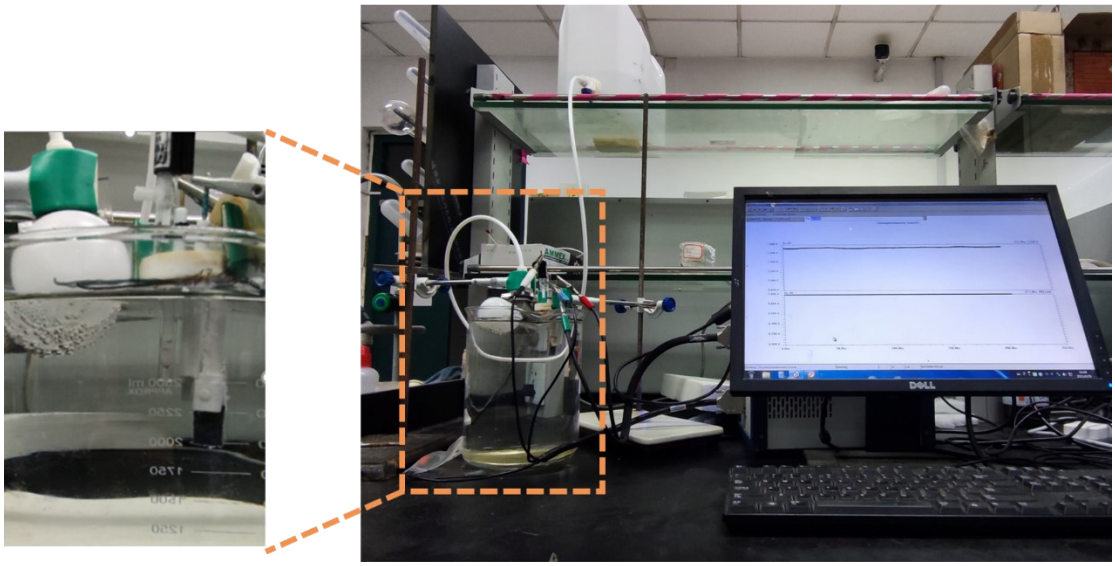

Fig. S12. Photograph of the setup with automatic rehydration system for a long-time stability test by chronopotentiometry at 500 mA cm^{-2}, using electrochemical workstation (Gamry Reference 3000, USA).

Fig. S13

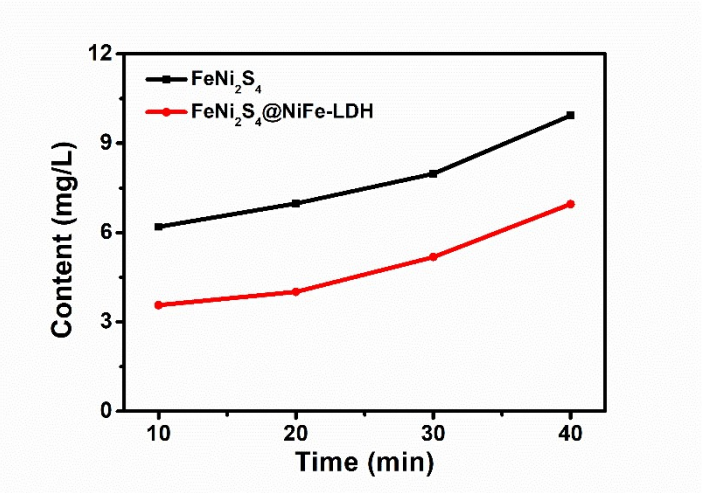

Fig. S13. S content in 1 M KOH of $FeNi_2S_4$@NiFe-LDH and $FeNi_2S_4$ under 100 mA cm^{-2}.

Fig. S14

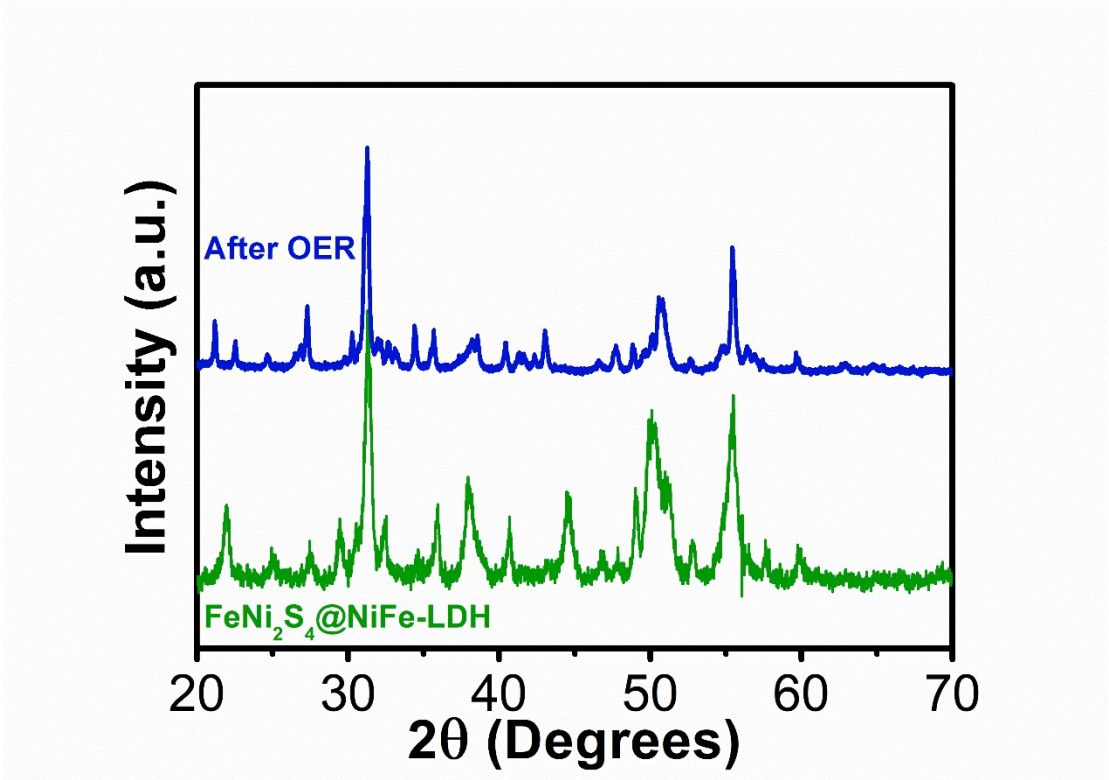

Fig. S14. XRD pattern of $FeNi_2S_4$@NiFe-LDH before and after long-term OER process.

Table S1. Elemental valence states of Fe and Ni species in the $FeNi_2S_4$@NiFe-LDH and their relative percentage ratios based on the deconvolution of peak areas.

Catalysts	Peak area ratio of Fe species (%)
	Fe^{2+} / Fe^{3+}
$FeNi_2S_4$	53.7 / 46.3
$FeNi_2S_4$@NiFe-LDH	26.6 / 73.4

Note: The ratios of elemental valence states calculated by the deconvoluted peak areas from XPS

Table S2. OER performances of $FeNi_2S_4$@NiFe-LDH and other reported electrocatalysts in alkaline media.

Catalyst	Electrolyte	η@j (mA cm^{-2})	Ref.
$FeNi_2S_4$@NiFe-LDH	**1 M KOH**	**238 mV@100** **283 mV@500** **306 mV@1000**	**This work**
Ta-NiFe LDH	1 M KOH	260 mV@50	[1]
Nb-NiFe-LDH	1 M KOH	242 mV@50	[2]
FeNi LDH	1 M KOH	240 mV@50	[3]
Ni(Fe)OOH–FeSx	1 M KOH	300 mV@50	[4]
S-NiFe-LDH-t-A	1 M KOH	270 mV@50	[5]
S-(Ni,Fe)OOH	1 M KOH	260 mV@50 281 mV@100	[6]
NiFeOH	1 M KOH	350 mV@100	[7]
F-NiFe-A	1 M KOH	240 mV@50	[8]
S-Ni_3FeN/NSG31.3	1 M KOH	360 mV@50	[9]
P-FeNiO/CNS	1 M KOH	300 mV@100	[10]
Ni_3Se_4@NiFe LDH/CFC	1 M KOH	250 mV@50 290 mV@100	[11]

Table S3. C_{dl} and ECSA surface area of all the as-obtained catalysts.

Catalyst	C_{dl} (mF)	ECSA (cm^2)
$FeNi_2S_4$@NiFe-LDH	248.41	6,210.25
$FeNi_2S_4$	172.41	4,310.25
NiFe-LDH	110.65	2,766.25
NiFe foam	26.92	673

References

[1] X. Wang, Y. Tuo, Y. Zhou, D. Wang, S. Wang and J. Zhang, Ta-doping triggered electronic structural engineering and strain effect in NiFe LDH for enhanced water oxidation, *Chem. Eng. J.*, 2021, **403**, 126297.

[2] Y.N. Zhou, F.L. Wang, S.Y. Dou, Z.N. Shi, B. Dong, W.L. Yu, H.Y. Zhao, F.G. Wang, J.F. Yu and Y.M. Chai, Motivating high-valence Nb doping by fast molten salt method for NiFe hydroxides toward efficient oxygen evolution reaction, *Chem. Eng. J.*, 2022, **427**, 131643.

[3] Q. Xiang, F. Li, W. Chen, Y. Ma, Y. Wu, X. Gu, Y. Qin, P. Tao, C. Song, W. Shang, H. Zhu, T. Deng and J. Wu, In situ vertical growth of Fe–Ni layered double-hydroxide arrays on Fe–Ni alloy foil: interfacial layer enhanced electrocatalyst with small overpotential for oxygen evolution reaction, *ACS Energy Lett.*, 2018, **3**, 2357–2365.

[4] H. Yang, L. Gong, H. Wang, C. Dong, J. Wang, K. Qi, H. Liu, X. Guo and B. Y. Xia, Preparation of nickel-iron hydroxides by microorganism corrosion for efficient oxygen evolution, *Nat. Commun.*, 2020, **11**, 5075.

[5] Y.N. Zhou, W.L. Yu, Y.N. Cao, J. Zhao, B. Dong, Y. Ma, F.L. Wang, R.Y. Fan, Y.L. Zhou and Y.M. Chai, S-doped nickel-iron hydroxides synthesized by room-temperature electrochemical activation for efficient oxygen evolution, Appl. Catal. B Environ. *Appl. Catal. B Environ.*, 2021, **292**, 120150.

[6] L. Yu, L. Wu, B. McElhenny, S. Song, D. Luo, F. Zhang, Y. Yu, S. Chen and Z. Ren, Ultrafast room-temperature synthesis of porous S-doped Ni/Fe (oxy)hydroxide

electrodes for oxygen evolution catalysis in seawater splitting, *Energy Environ. Sci.*, 2020, **13**, 3439–3446.

[7] Q. Zhou, Y. Chen, G. Zhao, Y. Lin, Z. Yu, X. Xu, X. Wang, H. K. Liu, W. Sun and S. X. Dou, Active-site-enriched iron-doped nickel/cobalt hydroxide nanosheets for enhanced oxygen evolution reaction, *ACS Catal.*, 2018, **8**, 5382–5390.

[8] Q. Xu, H. Jiang, X. Duan, Z. Jiang, Y. Hu, S. W. Boettcher, W. Zhang, S. Guo and C. Li, Fluorination-enabled reconstruction of NiFe electrocatalysts for efficient water oxidation, *Nano Lett.*, 2021, **21**, 492–499.

[9] C. Lai, M. Gong, Y. Zhou, J. Fang, L. Huang, Z. Deng, X. Liu, T. Zhao, R. Lin, K. Wang, K. Jiang, H. Xin and D. Wang, Sulphur modulated Ni_3FeN supported on N/S co-doped graphene boosts rechargeable/flexible Zn-air battery performance, *Appl. Catal. B Environ.*, 2020, **274**, 119086.

[10] Z. Liu, B. Tang, X. Gu, H. Liu and L. Feng, Selective structure transformation for NiFe/$NiFe_2O_4$ embedded porous nitrogen-doped carbon nanosphere with improved oxygen evolution reaction activity, *Chem. Eng. J.*, 2020, **395**, 125170.

[11] T. Zhang, L. Hang, Y. Sun, D. Men, X. Li, L. Wen, X. Lyu and Y. Li, Hierarchical hetero-Ni_3Se_4@NiFe LDH micro/nanosheets as efficient bifunctional electrocatalysts with superior stability for overall water splitting, *Nanoscale Horiz.*, 2019, **4**, 1132–1138.